

## Intense terahertz generation at low frequencies using an interdigitated ZnSe large aperture photoconductive antenna

X. Ropagnol,<sup>1,a)</sup> F. Blanchard,<sup>2</sup> T. Ozaki,<sup>1</sup> and M. Reid<sup>3</sup>

<sup>1</sup>*INRS-EMT, Advanced Laser Light Source, Université du Québec, Varennes, Québec J3X 1S2, Canada*

<sup>2</sup>*Department of Physics, McGill University, Montreal, Québec H3A 0G4, Canada*

<sup>3</sup>*Department of Physics, University of Northern British Columbia, Prince George, British Columbia V2N 4Z9, Canada*

(Received 8 July 2013; accepted 12 September 2013; published online 15 October 2013)

We demonstrate the generation of intense THz pulses at low frequencies, and THz pulse shaping, using a ZnSe interdigitated large aperture photoconductive antenna. We have experimentally measured a THz pulse energy of  $3.6 \pm 0.8 \mu\text{J}$ , corresponding to a calculated peak THz electric field of  $143 \pm 17 \text{ kV/cm}$ . We also used a binary phase mask instead of a traditional shadow mask with our interdigitated photoconductive antenna, which allows us to generate THz field profiles that range from a symmetric single-cycle THz pulse to an asymmetric half-cycle THz pulse.

© 2013 AIP Publishing LLC. [<http://dx.doi.org/10.1063/1.4825165>]

Recent developments in efficient and intense pulsed THz sources have made it possible to study fascinating nonlinear phenomena with tabletop set-ups,<sup>1,2</sup> such as the anisotropic mass of hot electrons in the non-parabolic conduction band of InGaAs<sup>3</sup> and the insulator-metal transition in VO<sub>2</sub>.<sup>4</sup> Tabletop, high-intensity THz sources have become available because of the development of techniques such as the tilted-pulse-front technique in LiNbO<sub>3</sub> and two-color plasma sources.<sup>5,6</sup> However, the first intense THz source was constructed with a GaAs large aperture photoconductive antenna (LAPCA).<sup>7</sup> This THz source is unique because it generates asymmetric half-cycle THz pulses with frequency components extending from 0.05 to above 1 THz. These relatively low THz frequencies are advantageous for achieving a strong ponderomotive potential, which can efficiently drive electrons in many nonperturbative phenomena such as above-threshold-ionization and high harmonic generation.<sup>8</sup>

It has been demonstrated that the THz electric field generated with a LAPCA is linearly dependent on the bias field.<sup>9</sup> As a consequence, large bias voltages are required to generate intense THz pulses from LAPCAs. GaAs is the most common material used for LAPCAs because of its attractive electrical and optical properties. However, its relatively low breakdown voltage limits the intensity of the THz pulses. ZnSe has a larger breakdown voltage than GaAs and thus when excited above the band gap, ZnSe LAPCAs have a higher potential to generate intense THz pulses.<sup>10</sup> ZnSe has a band gap of 2.7 eV and photo-excitation above the band gap requires optical pulses with wavelengths of 400 nm or shorter. On the other hand, working with conventional LAPCAs requires the manipulation of high voltage sources, which may be difficult to use. To avoid such difficulties, the interdigitated LAPCA is an alternative way to reduce the gap size while maintaining a large aperture for illumination, which is essential in order to generate intense THz pulses. It has been demonstrated that such structures on GaAs LAPCAs can generate relatively high fields with very high

optical to THz energy conversion efficiency.<sup>11</sup> In this Letter, we present the results of our work on interdigitated ZnSe LAPCAs to generate intense low frequency THz pulses. We used different masks (shadow and binary phase masks) with our interdigitated structure, allowing us to control the temporal profile of the generated THz pulse. This technique allows one to easily switch between the generation of an asymmetric half-cycle THz pulse and a symmetric single-cycle THz pulse.<sup>12</sup> Controlling the temporal pulse shape is expected to be useful for many applications such as the control of the orientation of polar molecules and the control of the dynamics of electrons in mesoscopic structures.<sup>13,14</sup>

Here, we report the generation of  $3.6 \pm 0.8 \mu\text{J}$  THz pulse energies from an interdigitated ZnSe LAPCA with a temporal pulse shape that can be varied from a half-cycle to a single-cycle THz pulse using binary phase and shadow masks. This THz pulse energy is 4.5 times higher than previously reported using LAPCAs.<sup>7</sup> When combined with the capability for pulse shaping, this intense THz source is expected to be a valuable tool for studying applications in nonlinear THz-matter interactions.

In this work, we used a  $5.5 \text{ cm}^2$  aperture ZnSe antenna, which is composed of 24 identical antennas with an electrode gap spacing of  $600 \mu\text{m}$ , and an electrode length and width of  $22 \text{ mm}$  and  $400 \mu\text{m}$ , respectively. The contacts were made using  $30 \text{ nm}$  of Cr and  $150 \text{ nm}$  of Pt. The  $600 \mu\text{m}$  gap size is large enough to ensure operation in the THz-field-screening regime, so that the radiated THz field is not limited by space-charge-screening.<sup>15</sup> The electrode pattern was fabricated using conventional photolithography. The bias field was provided using a high-voltage pulsed generator, which can generate  $7 \text{ kV}$  pulses with  $20 \text{ ns}$  duration. The phase mask is composed of 12 quartz plates that are  $1 \text{ mm}$  wide and  $25 \text{ mm}$  long. Two different thicknesses of quartz were used,  $0.65$  and  $1 \text{ mm}$ . The shadow mask is also composed of 12 quartz plates, but they have been painted in black to make them opaque. The principle of a binary phase mask for single-cycle THz pulse generation has been previously reported.<sup>12</sup> Figure 1 shows a schematic diagram of the ZnSe antenna covered with a binary phase mask and a shadow

<sup>a)</sup>Author to whom correspondence should be addressed. Electronic mail: ropagnol@emt.inrs.ca. Telephone: +1-514-228-6979.

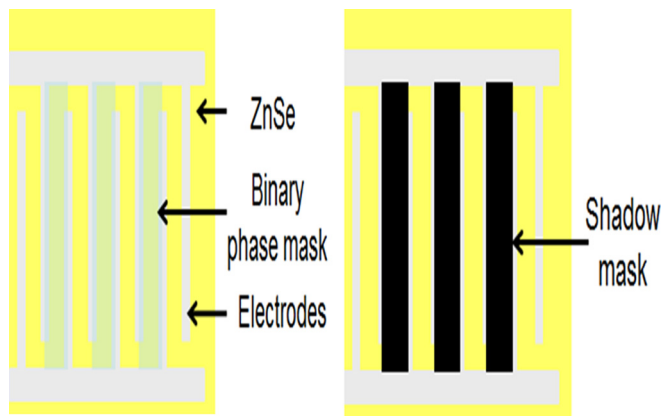


FIG. 1. Schematic diagram of the interdigitated ZnSe antenna covered with a binary phase mask (left side, transparent quartz masks) and a shadow mask (right side, black painted opaque quartz).

mask. Two different amplified Ti:sapphire lasers were used to excite the LAPCA. The first laser delivers 3.5 mJ, 35 fs pulses at 2.5 kHz repetition rate and at 800 nm wavelength. The second laser delivers 270 mJ, 35 fs pulses at 10 Hz repetition rate at 800 nm. The 10 Hz laser was used in order to illuminate the entire area of the interdigitated ZnSe LAPCA with sufficient fluence at 400 nm to observe saturation behavior, and generate the highest pulse energies possible. The 2.5 kHz laser has a limited fluence at 400 nm due to the limited SHG conversion efficiency of the  $\beta$ -barium borate (BBO) crystal, but was used to investigate the general behavior of the source. The optical pump beam size (full-width at  $1/e^2$ ) on the emitter was 0.8 cm when using the 2.5 kHz laser,

and 3.5 cm with the 10 Hz laser (full illumination of the antenna). The THz radiation was detected in three different ways: using a pyroelectric detector (with the 10 Hz laser), using electro-optic (E.O.) sampling in ZnTe (with the 2.5 kHz laser), and using an infrared camera (with the 10 Hz laser). The THz pulses were focused on to the detectors using a single  $90^\circ$  off-axis parabolic mirror with an F-number of 1 (for energy detection and image capture) or 2 (for electric field detection).

Figure 2(a) shows the pulse shape of the THz radiation from an interdigitated ZnSe LAPCA with a shadow mask or binary phase mask, with two thicknesses at 0.65 mm or 1 mm. The THz electric field was detected using electro-optic sampling in a 1 mm thick [110] ZnTe crystal.<sup>16</sup> The shadow mask (blue curves) generates an asymmetric half-cycle THz pulse. The THz waveform becomes symmetric and single-cycle with the 1 mm thick binary phase mask (red curve). Changing the mask thickness from 1 mm to 0.65 mm reduces the THz pulse duration (black curve). A reduction in the negative peak of the THz peak electric field between the 0.65 mm and the 1 mm mask is observed. This reduction is a consequence of the overlapping in time of the positive and negative polarity half-cycle THz pulse from neighboring antennas when using the 0.65 mm mask. The Figure 2(b) shows the power spectrum of the radiated THz electric field obtained with the 1 mm binary mask and the shadow mask. Both spectra extend up to approximately 3.5 THz. However, the main frequency components lie between 0.05 THz and 1 THz. This spectrum is unique to the LAPCA in comparison with the other intense THz sources.

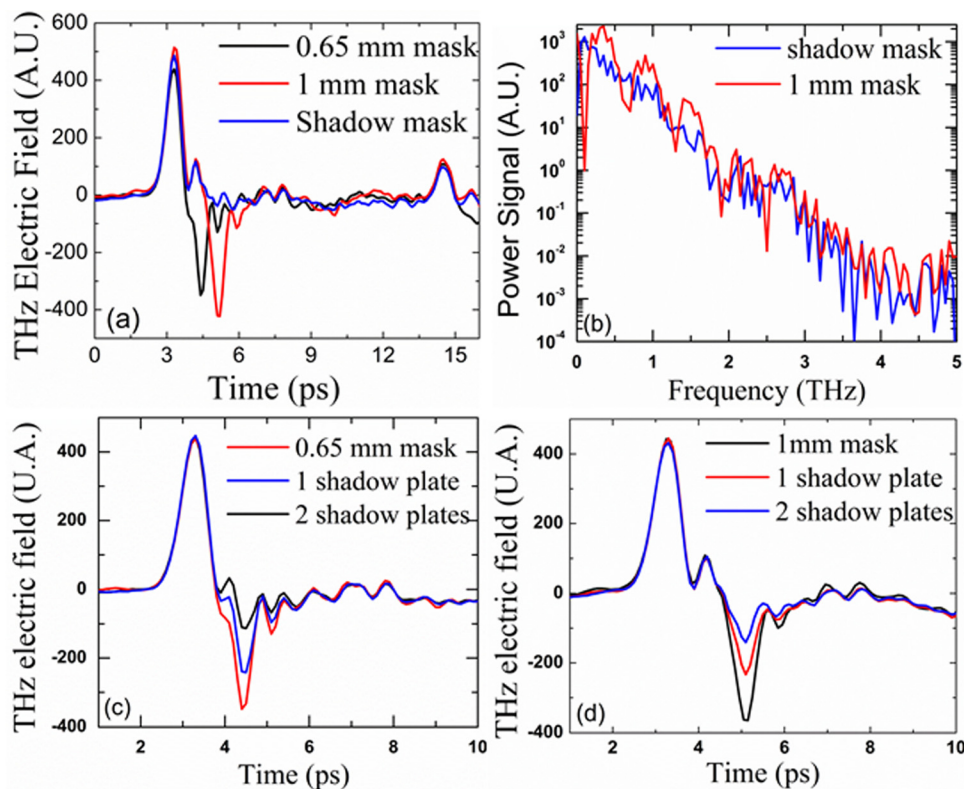


FIG. 2. (a) THz pulses shapes generated from the ZnSe interdigitated LAPCA excited at 400 nm with a fluence of  $0.2 \text{ mJ/cm}^2$ , at a bias field of 10 kV/cm with 0.65 mm and 1 mm binary mask and a shadow mask. (b) shows the power spectrum with a shadow mask (blue line) and the 1 mm binary mask (red line). (c) and (d) show the THz pulse shapes obtained with the 0.65 mm (c) and the 1 mm (d) binary mask on the ZnSe interdigitated LAPCA. The THz pulse shaping is accomplished by inserting combinations of shadow and phase masks. The antenna is excited at 400 nm with  $0.2 \text{ mJ/cm}^2$  fluence at bias field of 10 kV/cm.

Figures 2(c) and 2(d) show the THz pulse shape generated by the interdigitated ZnSe LAPCA with 0.65 mm (c) and 1 mm (d) binary mask, but replacing some of the phase masks with shadow plates. The shadow plates are identical to the ones that have been used to make the shadow mask. By doing so, we could vary the magnitude of the negative peak. The results presented in Figures 2(c) and 2(d) were obtained using the 2.5 kHz laser with E.O. sampling. The optical excitation beam size on the emitter was approximately 0.8 cm. As a consequence, inserting one shadow plate in the binary phase mask induces a  $\sim 30\%$  reduction of the negative peak THz electric field. Figures 2(c) and 2(d) show that by combining phase and shadow masks on an interdigitated ZnSe LAPCA, one can vary the THz pulse shape between an asymmetric half-cycle and a symmetric single-cycle pulse.

Figure 3(a) shows an image captured with a ferroelectric infrared camera (Electro Physics model PV320-L2Z) of a focused THz pulse generated by the interdigitated ZnSe LAPCA excited with  $0.55 \text{ mJ/cm}^2$  and biased at  $35 \text{ kV/cm}$ . The results in Figure 3 were obtained using the 10 Hz laser, and the THz beam was collected with a  $2''$  diameter,  $2''$  focal length  $90^\circ$  off-axis parabolic mirror. Assuming a Gaussian profile, the spot size of the THz beam (intensity) at the focus was found to be  $3.2 \times 2.9 \text{ mm}$  full-width at  $1/e^2$  maximum, which gives a total elliptical THz spot area of  $7.3 \text{ mm}^2$ . The THz beam spot size seen here is large compared to the typical THz beam spot size obtained using other intense THz sources.<sup>17,18</sup> The reason for this is the higher fraction of low

THz frequency components in the pulse, leading to a larger diffraction-limited spot size.

Figure 3(b) shows the variation of the THz energy and (c) the square root of the THz energy as a function of the optical excitation fluence. The THz energy was detected with a pyroelectric detector (Gentec I-BNC). This detector has a typical sensitivity of  $140 \text{ kV/W}$  at  $10.6 \mu\text{m}$  wavelength. However, calibration of the response in the THz frequency range was carried out by cross-calibration with a Coherent-Moletron pyroelectric detector, previously calibrated in the THz frequency range.<sup>19</sup> The calibration gives a sensitivity of  $10 \mu\text{W/V}$ . We note that the apertures of both pyroelectric detectors were  $2 \text{ mm}$ , which is smaller than the THz spot size. Therefore, all energy measurements have been corrected (increased) by a factor of 1.6, accounting for the THz spot size dimensions relative to the detection aperture.

The THz energy as a function of the excitation fluence was compared from our LAPCA using a binary phase mask and a shadow mask. The THz energy using the  $1 \text{ mm}$  binary phase mask is larger by a factor of 1.7. This factor is lower than 2, which is the maximum difference that we can expect.<sup>12</sup> This difference can be explained by the imperfect alignment of the mask on the interdigitated structure. The THz energy grows rapidly for low excitation fluences. Saturation of the THz energy with fluence is observed, which is expected when LAPCAs operate in the THz-field-screening regime.<sup>20</sup> The square root of the THz energy (proportional to the peak electric field) is plotted against the excitation fluence

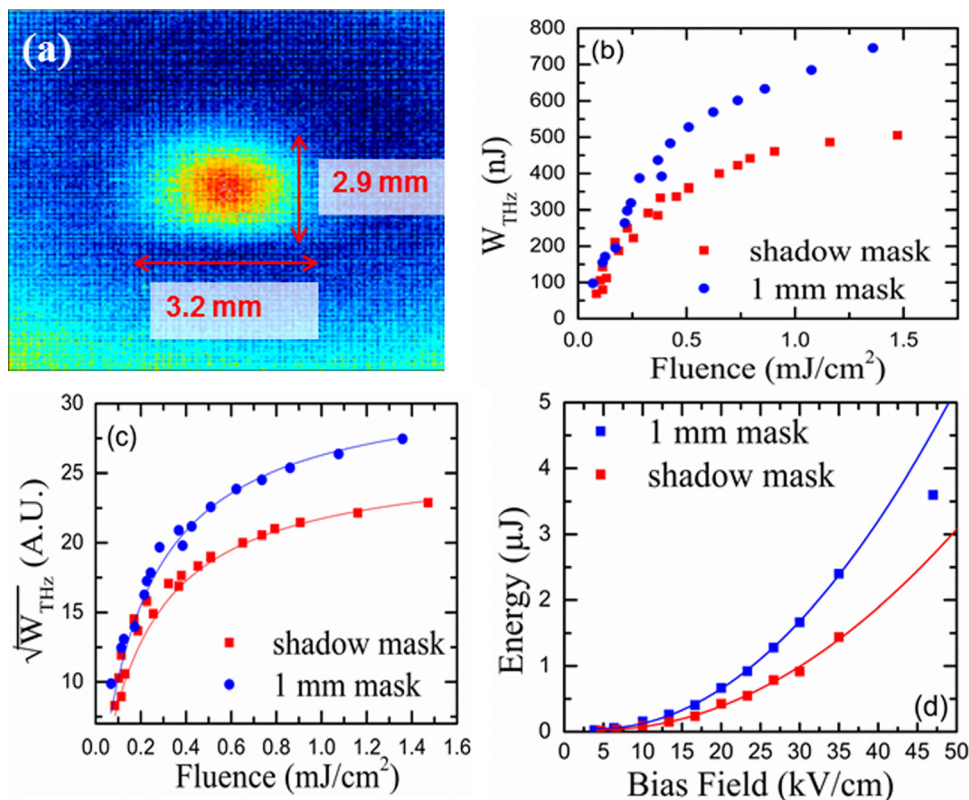


FIG. 3. (a) Real-time image of the THz pulse at the focus position captured with a ferroelectric infrared camera. The interdigitated ZnSe LAPCA was excited at  $0.55 \text{ mJ/cm}^2$  at  $400 \text{ nm}$  and bias at  $35 \text{ kV/cm}$ . (b) THz energy ( $W_{\text{THz}}$ ) and square root of the THz energy (c) as a function of excitation fluence emitted by the interdigitated ZnSe LAPCA excited at  $400 \text{ nm}$  and biased at  $20 \text{ kV/cm}$ . (d) THz energy as a function of the bias field emitted by the interdigitated ZnSe LAPCA excited at  $400 \text{ nm}$  with a fluence of  $0.55 \text{ mJ/cm}^2$  with the  $1 \text{ mm}$  mask (blue) and the shadow mask (red). The THz energy is detected using a pyroelectric detector.

in Figure 3(c). The data were fit using Eq. (1) below, which allows the saturation fluence of the antenna to be determined

$$\sqrt{W_{THz}} \propto \beta \left( \frac{F}{F + F_{sat}} \right). \quad (1)$$

Here,  $W_{THz}$  is the THz pulse energy,  $F$  is the optical excitation fluence,  $F_{sat}$  is the saturation fluence, and  $\beta$  is a constant that depends on the bias field. From Figure 3(c), we observe the saturation of the square root of the THz energy with the two masks. From the fitted curve, we extract the measured saturation fluence to be  $0.22 \pm 0.02$  mJ/cm<sup>2</sup>.

Figure 3(d) shows the variation of the THz energy as a function of the bias field when the ZnSe antenna is excited at  $0.55$  mJ/cm<sup>2</sup>. As expected, a quadratic relationship between the THz energy and the bias field is observed up to  $35$  kV/cm for the two masks, consistent with the operation of a LAPCA.<sup>9</sup> The maximum THz energy is obtained with the  $1$  mm phase mask when the antenna is biased at  $47$  kV/cm. A maximum voltage of  $2.3 \pm 0.5$  V was measured, which corresponds to a THz pulse energy of  $2.3 \pm 0.5$   $\mu$ J. Applying the correction factor discussed above to take into account the smaller size of the pyroelectric detector area, our measurements correspond to a pulse energy of  $3.6 \pm 0.8$   $\mu$ J, which is  $4.5$  times larger than previously reported with a GaAs LAPCA.<sup>7</sup> Interestingly, the quadratic scaling does not appear to hold up to the highest applied bias fields. If the quadratic relationship remained valid, an even larger THz pulse energy would be expected. This sub-quadratic scaling at high bias fields is attributed primarily to the presence of strong corona discharges that became problematic at large applied bias fields. The corona discharge is also responsible for the high margin of error on the THz pulse energy at  $47$  kV/cm. This THz pulse energy was generated using a  $400$  nm laser pulse with energy of  $5.3$  mJ at  $10$  Hz repetition rate. The maximum optical-to-THz conversion efficiency for this source under these operating conditions is  $6.8 \times 10^{-4}$ . This THz efficiency is low in comparison to the efficiency of GaAs LAPCA.<sup>7</sup> This difference is the result of the difference in the carrier mobilities between the GaAs and ZnSe crystals.<sup>12</sup> The second harmonic generation efficiency was not taken into account in our calculation. The equivalent THz peak electric field is estimated using the equation<sup>21</sup>

$$E_0 = \frac{\eta_0 W_{THz}}{\sqrt{A \int g^2(t) dt}}. \quad (2)$$

Here,  $W_{THz}$  is the THz energy,  $\eta_0$  is the free impedance,  $A$  is the intensity area of the THz spot size, and  $g(t)$  is the normalized temporal shape of the THz electric field that we extract from Figure 1. The  $3.6 \pm 0.8$   $\mu$ J THz pulse generated with the  $1$  mm mask has a calculated equivalent focused THz

peak electric field of  $143 \pm 17$  kV/cm. A larger applied bias field would have enhanced the radiated THz peak electric field, but in these experiments, the bias field was limited by air breakdown.

In conclusion,  $3.6 \pm 0.8$   $\mu$ J THz pulses were generated using an interdigitated ZnSe LAPCA with a binary phase mask. The focused THz intensity spot size area was  $7.3$  mm<sup>2</sup> and was close to the diffraction limit. The equivalent THz peak electric field was estimated to be  $143 \pm 17$  kV/cm. This source is unique compared to traditional high-intensity THz sources because of the predominance of relatively low frequency components, which are ideally suited to generate a large ponderomotive potential useful for nonlinear THz-matter interactions. Further, the temporal profile of the THz field radiated from this source can be tailored to specific shapes between single- and half-cycle THz pulses, which may also be useful for future high-intensity studies.

- <sup>1</sup>L. Razzari, F. H. Su, G. Sharma, F. Blanchard, A. Ayesheshim, H.-C. Bandulet, R. Morandotti, J.-C. Kieffer, T. Ozaki, M. Reid, and F. A. Hegmann, *Phys. Rev. B* **79**, 193204 (2009).
- <sup>2</sup>M. C. Hoffmann, J. Hebling, H. Y. Hwang, K.-L. Yeh, and K. A. Nelson, *Phys. Rev. B* **79**, 161201 (2009).
- <sup>3</sup>F. Blanchard, D. Golde, F. H. Su, L. Razzari, G. Sharma, R. Morandotti, T. Ozaki, M. Reid, M. Kira, S. W. Koch, and F. A. Hegmann, *Phys. Rev. Lett.* **107**, 107401 (2011).
- <sup>4</sup>M. Liu, H. Y. Hwang, H. Tao, A. C. Strikwerda, K. Fan, G. R. Keiser, A. J. Sternbach, K. G. West, S. Kittiwatanakul, J. Lu, S. A. Wolf, F. G. Omenetto, X. Zhang, K. A. Nelson, and R. D. Averitt, *Nature* **487**, 345 (2012).
- <sup>5</sup>J. A. Fülöp, L. Pálfalvi, S. Klingebiel, G. Almasi, F. Krausz, S. Karsch, and J. Hebling, *Opt. Lett.* **37**, 557 (2012).
- <sup>6</sup>K. Y. Kim, J. H. Glowina, A. J. Taylor, and G. Rodriguez, *IEEE J. Quantum Electron.* **48**, 797 (2012).
- <sup>7</sup>D. You, R. R. Jones, and P. H. Bucksbaum, *Opt. Lett.* **18**, 290 (1993).
- <sup>8</sup>H. Hirori and K. Tanaka, *IEEE J. Sel. Top. Quantum Electron.* **19**, 8401110 (2013).
- <sup>9</sup>J. T. Darrow, X.-C. Zhang, D. H. Auston, and J. D. Morse, *IEEE J. Quantum Electron.* **28**, 1607 (1992).
- <sup>10</sup>X. Ropagnol, R. Morandotti, T. Ozaki, and M. Reid, *IEEE Photon. J.* **3**, 174 (2011).
- <sup>11</sup>M. Beck, H. Schäfer, G. Klatt, J. Demsar, S. Winnerl, M. Helm, and T. Dekorsy, *Opt. Express* **18**, 9251 (2010).
- <sup>12</sup>X. Ropagnol, R. Morandotti, T. Ozaki, and M. Reid, *Opt. Lett.* **36**, 2662 (2011).
- <sup>13</sup>A. Matos-Abiague and J. Berkdar, *Phys. Rev. A* **68**, 063411 (2003).
- <sup>14</sup>A. Matos-Abiague and J. Berkdar, *Phys. Rev. Lett.* **94**, 166801 (2005).
- <sup>15</sup>D. S. Kim and D. S. Citrin, *Appl. Phys. Lett.* **88**, 161117 (2006).
- <sup>16</sup>Q. Wu, M. Litz, and X.-C. Zhang, *Appl. Phys. Lett.* **68**, 2924 (1996).
- <sup>17</sup>H. Hirori, A. Doi, F. Blanchard, and K. Tanaka, *Appl. Phys. Lett.* **98**, 091106 (2011).
- <sup>18</sup>M. Clerici, M. Pecianti, B. E. Schmidt, L. Caspani, M. Shalabi, M. Giguère, A. Lotti, A. Couairon, F. Légaré, T. Ozaki, D. Faccio, and R. Morandotti, *Phys. Rev. Lett.* **110**, 253901 (2013).
- <sup>19</sup>F. Blanchard, L. Razzari, H. C. Bandulet, G. Sharma, R. Morandotti, J. C. Kieffer, T. Ozaki, M. Reid, H. F. Tiedje, H. K. Haugen, and F. A. Hegmann, *Opt. Express* **15**, 13212 (2007).
- <sup>20</sup>G. Rodriguez and A. J. Taylor, *Opt. Lett.* **21**, 1046 (1996).
- <sup>21</sup>M. D. Thomson, M. Kress, T. Löffler, and H. G. Roskos, *Laser Photonics Rev.* **1**, 349 (2007).

Applied Physics Letters is copyrighted by the American Institute of Physics (AIP).  
Redistribution of journal material is subject to the AIP online journal license and/or AIP  
copyright. For more information, see <http://ojps.aip.org/aplo/aplcr.jsp>